Research Square

Preprints are preliminary reports that have not undergone peer review.
They should not be considered conclusive, used to inform clinical practice,
or referenced by the media as validated information.

STMN2 promotes osteogenic differentiation and bone formation in mouse bone marrow mesenchymal stem cells via the Wnt signaling pathway

Xiaoping Jin
Chengdu University of Traditional Chinese Medicine
Jun Cheng
Chengdu Fifth People's Hospital
Shuxing Xing
Chengdu Fifth People's Hospital
Zhangzhen Du
Dzzupu@163.com

Chengdu Fifth People's Hospital

Article

Keywords: STMN2, Bone marrow mesenchymal stem cells, Osteogenic differentiation, Wnt signaling pathway, Bone regeneration

Posted Date: October 30th, 2026

DOI: https://doi.org/10.21203/rs.3.rs-11237883/v1

License: This work is licensed under a Creative Commons Attribution 4.0 International License.
Read Full License

Additional Declarations: No competing interests reported.

STMN2 promotes osteogenic differentiation and bone formation in mouse bone marrow mesenchymal stem cells via the Wnt signaling pathway

Xiaoping Jin[1,2] Jun Cheng[2], Shuxing Xing[2]*, Zhangzhen Du[2]**.

1.Chengdu University of Traditional Chinese Medicine, Chengdu 611137, China.

2. Department of Orthopaedics, Chengdu Fifth People's Hospital, Chengdu 611130, China.

*Corresponding author at: Department of Orthopaedics, Chengdu Fifth People's Hospital, Chengdu 611130, China.

**Corresponding author at: Department of Orthopaedics, Chengdu Fifth People's Hospital, Chengdu 611130, China.

E-mail addresses: 3296315867@qq.com(S. Xing), dzzupu@163.com(Z. Du)

Highlights

STMN2 was upregulated during osteogenic differentiation of mouse BMSCs.

STMN2 overexpression promoted BMSC proliferation, migration, and osteogenic differentiation.

STMN2 knockdown attenuated BMSC proliferation, migration, and osteogenesis.

STMN2 overexpression enhanced bone regeneration in mouse calvarial defects.

Wnt/β-catenin signaling mediated STMN2-promoted osteogenesis, identifying STMN2 as a potential therapeutic target.

Abstract

Stathmin 2 (STMN2) is a microtubule-associated protein whose role in the osteogenic differentiation of bone marrow mesenchymal stem cells (BMSCs) remains unclear. This study aimed to investigate the regulatory role of STMN2 in osteogenic differentiation and bone regeneration in mouse BMSCs. BMSCs were transduced with lentiviral constructs for STMN2 overexpression, STMN2 knockdown, or negative control. Proliferation, migration, ALP activity, mineralization, and expression of RUNX2, BMP2, BGLAP, and COL1A2 were assessed. Transduced BMSCs were implanted into calvarial defects and evaluated by micro-CT, H&E staining, and immunohistochemistry; transcriptome sequencing and Wnt/β-catenin agonist rescue experiments were also performed. STMN2 was upregulated during osteogenesis. Overexpression promoted proliferation, migration, osteogenic differentiation, and in vivo bone formation, whereas knockdown attenuated these effects. A Wnt agonist partially rescued the osteogenic defect in STMN2-knockdown BMSCs. In conclusion, STMN2 promotes the osteogenic differentiation of

mouse BMSCs and enhances bone regeneration, identifying it as a potential therapeutic target.

Keywords: STMN2; Bone marrow mesenchymal stem cells; Osteogenic differentiation; Wnt signaling pathway; Bone regeneration.

1. Introduction

Repair of bone defects remains a major challenge in orthopedics, with common etiologies including trauma, infection, tumor resection, and congenital deformities[1]. Although autologous bone grafting is widely regarded as the "gold standard" for bone defect repair, its clinical application is limited by the limited donor site source, the need for additional bone harvesting surgery (secondary surgical trauma), and donor site complications[2][3][4]. Consequently, there is considerable interest in developing novel bone regeneration strategies based on stem cell tissue engineering. Bone marrow mesenchymal stem cells (BMSCs) are considered promising "seed cells" for bone tissue engineering due to their robust osteogenic differentiation potential, immunomodulatory and paracrine activities that regulate the bone microenvironment, and relative ease of isolation [5][6]. A thorough understanding of the molecular regulatory networks governing BMSC osteogenic differentiation and the identification of key signaling pathways and effector molecules are crucial for optimizing BMSC-based bone regeneration strategies.

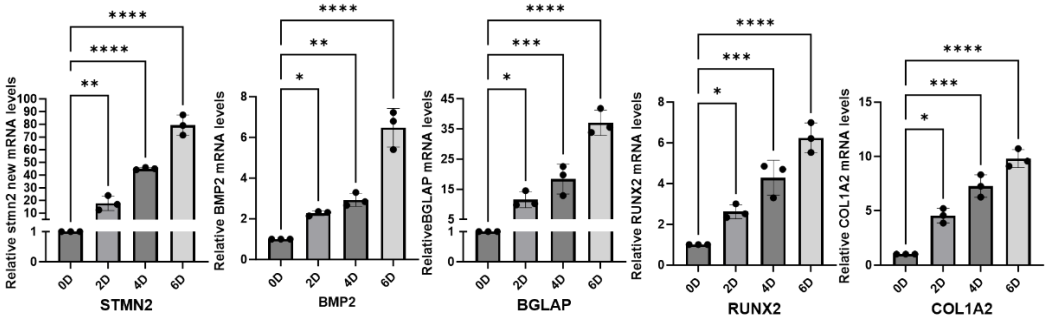
Stathmin 2 (STMN2/SCG10), a member of the stathmin family, is highly expressed in the nervous system, particularly in motor neurons. Through its microtubule-depolymerizing and dynamics-regulating activities, STMN2/SCG10 participates in neuronal differentiation, axon growth, and regeneration, and is closely associated with synaptic plasticity and axon guidance[7][8][9]. Notably, Kumar et al. identified stathmin in osteoblasts of human and rat origin, suggesting a potential role for this protein family in osteoblast regulation[10]. Chiellini et al. reported that STMN2 mRNA and protein levels increased during osteogenic differentiation of human MSCs[11].Furthermore, Tuerlings et al., using RNA sequencing of bone tissue from osteoarthritis patients, found that STMN2 was significantly upregulated in osteoarthritic samples compared to controls[12]. Despite these clues, the biological function of STMN2 in BMSC osteogenic differentiation and bone regeneration remains unexplored, with limited reports available. To further investigate this, we analyzed the public dataset "Transcriptome expression of human bone marrow mesenchymal stem cells (hBMSC) during osteogenesis" (GSE178679) from the GEO database. This analysis revealed that STMN2 was significantly upregulated during osteogenesis. Consistent with this, our preliminary experiments showed a time-dependent increase in STMN2 expression during osteogenic induction of BMSCs, suggesting that STMN2 may play a regulatory role in this process.

Based on this background, the present study aims to systematically investigate the regulatory effect of STMN2 on the osteogenic differentiation of mouse BMSCs and its impact on bone regeneration in vivo. By constructing STMN2 overexpression and knockdown lentiviral vectors, we evaluated the effects of STMN2 on BMSC proliferation, osteogenic phenotype, expression of osteogenic-related genes, and new bone formation in a mouse calvarial defect model. This study seeks to provide new experimental evidence for the molecular regulation of bone regeneration and to explore potential therapeutic targets for bone metabolic diseases.

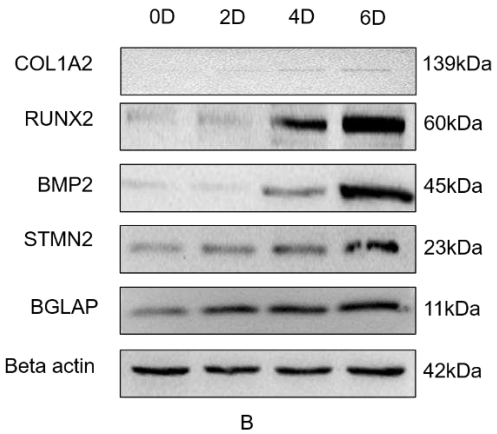
2. Results

2.1. STMN2 is upregulated during osteogenic differentiation

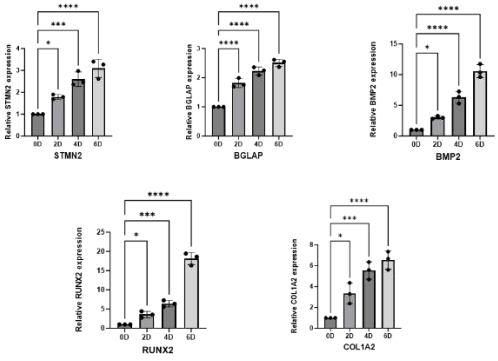
To examine the role of STMN2 in osteogenic differentiation, BMSCs were cultured in osteogenic medium, and STMN2 expression was analyzed. qRT-PCR results (Fig. 1A) showed that STMN2 expression was upregulated in a time-dependent manner (days 0–6), as were the osteogenic marker genes BMP2, BGLAP, RUNX2, and COL1A2. Western blot analysis confirmed these findings at the protein level (Fig. 1B, C). Consistent with these data, analysis of the GEO dataset GSE178679 revealed that STMN2 was significantly upregulated during osteogenesis in human BMSCs (Fig. 1D). Furthermore, research conducted by Tuerlings et al[12]. indicates that STMN2 was significantly upregulated in osteoarthritis samples compared with controls (Fig. 1E). These results suggest that STMN2 may be involved in the osteogenic differentiation process.



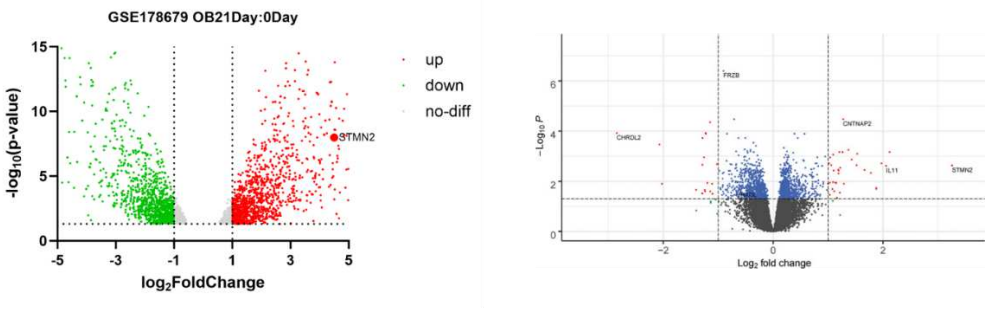
A



B



C



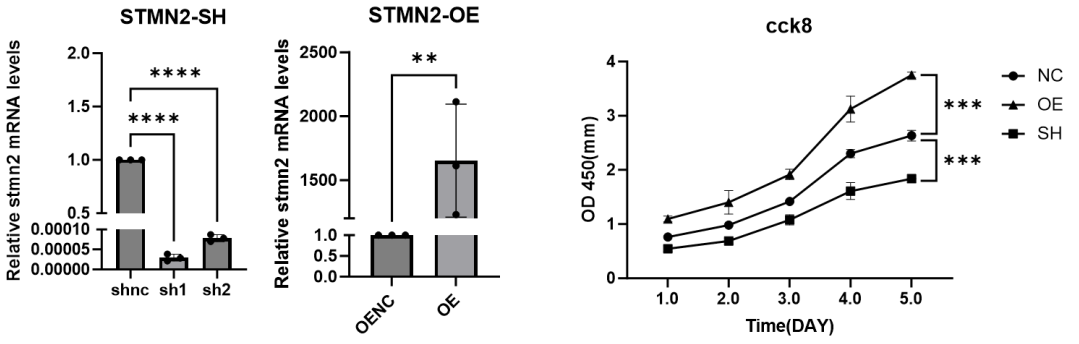
D E

Figure 1. STMN2 expression is upregulated during osteogenic differentiation of BMSCs.

BMSCs were cultured in osteogenic induction medium for the indicated durations. (A) qRT-PCR analysis of mRNA levels of STMN2 and the osteogenic marker genes *BMP2, BGLAP, RUNX2,* and *COL1A2*. (B, C) Representative Western blots (B) and densitometric quantification (C) of STMN2, BMP2, BGLAP, RUNX2, and COL1A2 protein levels. β-actin served as the internal loading control. (D) Differential gene expression analysis of STMN2 in the GEO dataset GSE178679 during osteogenic differentiation of human BMSCs. (E) STMN2 expression in osteoarthritis (OA) samples compared with control samples from the GEO dataset(Quoted from[12]). Data are presented as mean ± SD (n = 3 per group). *p < 0.05, **p < 0.01, ***p < 0.001, ****p < 0.0001.

2.2. STMN2 promotes cell proliferation and migration

To further investigate the role of STMN2 in osteogenesis, BMSCs were transduced with lentiviral vectors for STMN2 overexpression, knockdown, or negative control. Transduction efficiency was confirmed by qRT-PCR (Fig. 2A). CCK-8 assay results showed that, compared with the NC group, cell proliferation was significantly decreased in the knockdown group and increased in the overexpression group (Fig. 2B). Wound-healing assay results revealed that STMN2 overexpression enhanced cell migration, while knockdown reduced it (Fig. 2C–F). These findings indicate that STMN2 promotes BMSC proliferation and migration.



A B

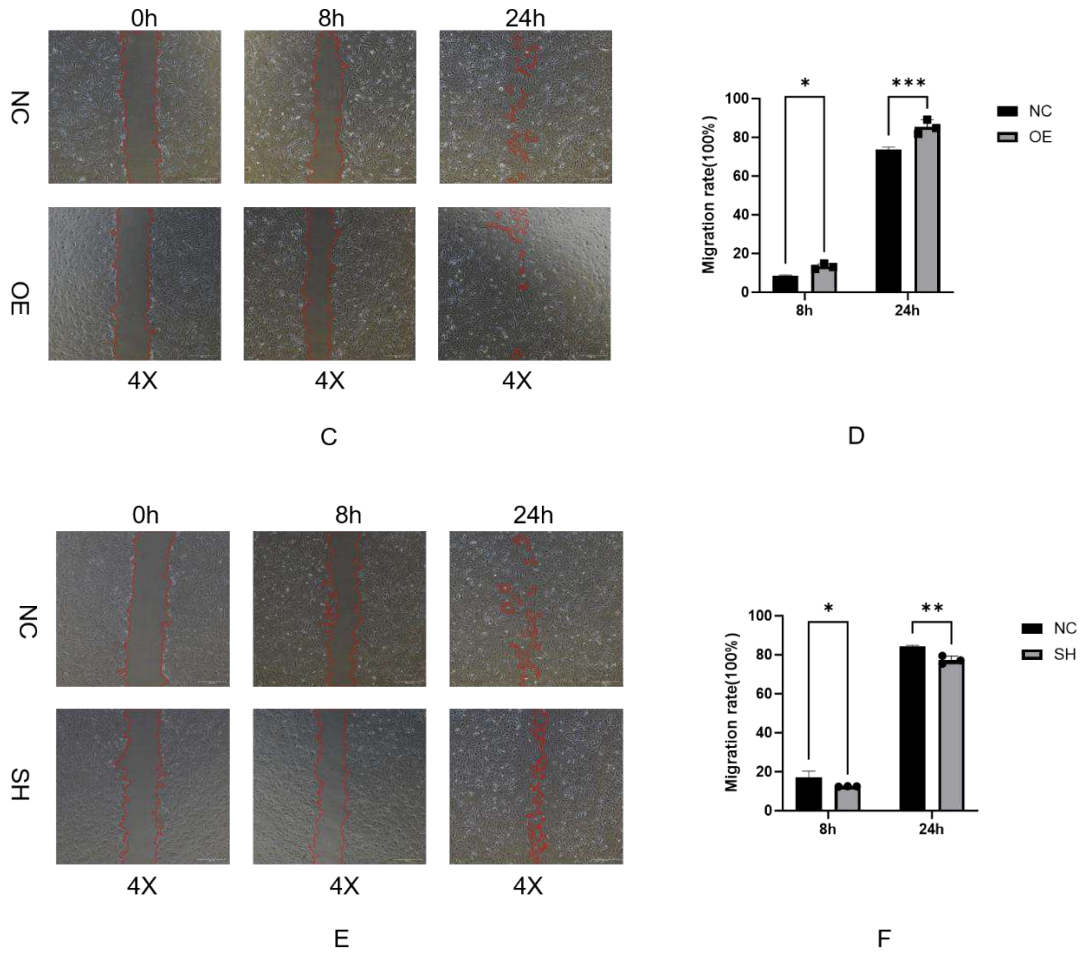
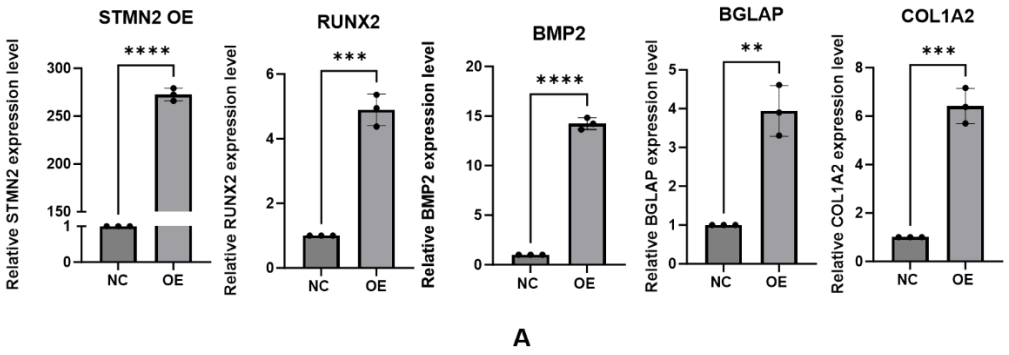


Figure 2. STMN2 promotes BMSC proliferation and migration in vitro.
BMSCs were transduced with lentiviral vectors for STMN2 overexpression (OE-STMN2), knockdown (SH-STMN2), or negative controls (OE-NC and SH-NC). (A) qRT-PCR validation of STMN2 expression levels 48 h post-transduction. (B) Cell viability was assessed by the CCK-8 assay on days 1–5 post-seeding. (C, E) Representative images of wound-healing assays at 0, 8, and 24 h post-scratching (scale bar: 500 μm). (D, F) Quantitative analysis of relative wound width, normalized to the 0-h time point. Data are presented as mean ± SD (n = 3 per group). *p < 0.05, **p < 0.01, ***p < 0.001.

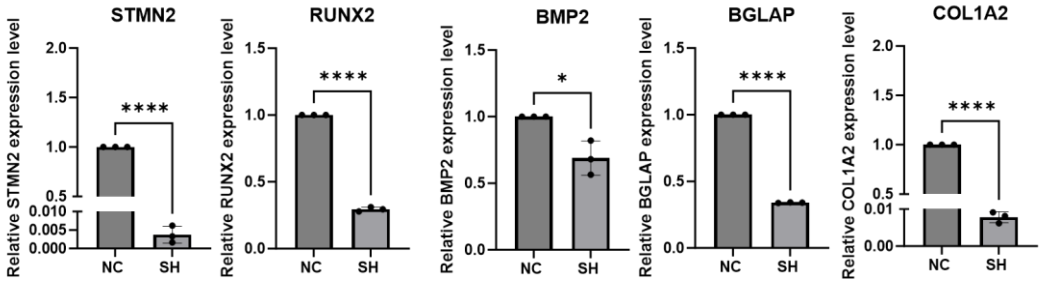
2.3. STMN2 enhances osteoblast differentiation and matrix mineralization in vitro

The effect of STMN2 on osteogenic differentiation was further investigated. qRT-PCR, Western blotting, and immunofluorescence staining showed that the mRNA and protein levels of BMP2, BGLAP, RUNX2, and COL1A2 were significantly increased in the STMN2-overexpressing group (Fig. 3A, C, E) but decreased in the knockdown group (Fig. 3B, D, F) compared with controls. ALP staining and activity assays (Fig. 3G, H) and ARS staining (Fig. 3I, J) demonstrated that STMN2 overexpression significantly enhanced ALP activity and calcium deposition, whereas STMN2

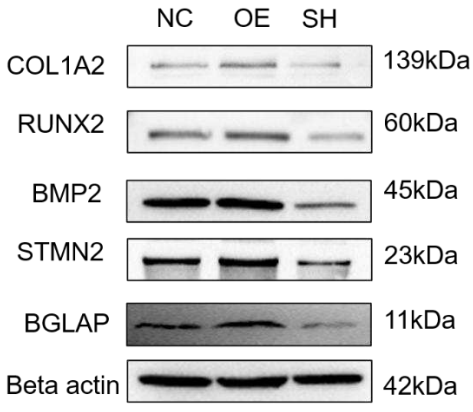
knockdown attenuated these effects. Collectively, these results demonstrate that STMN2 positively regulates osteoblast differentiation and mineralization.



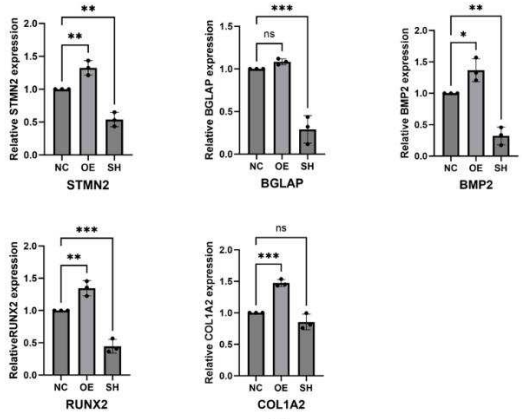
A



B



C



D

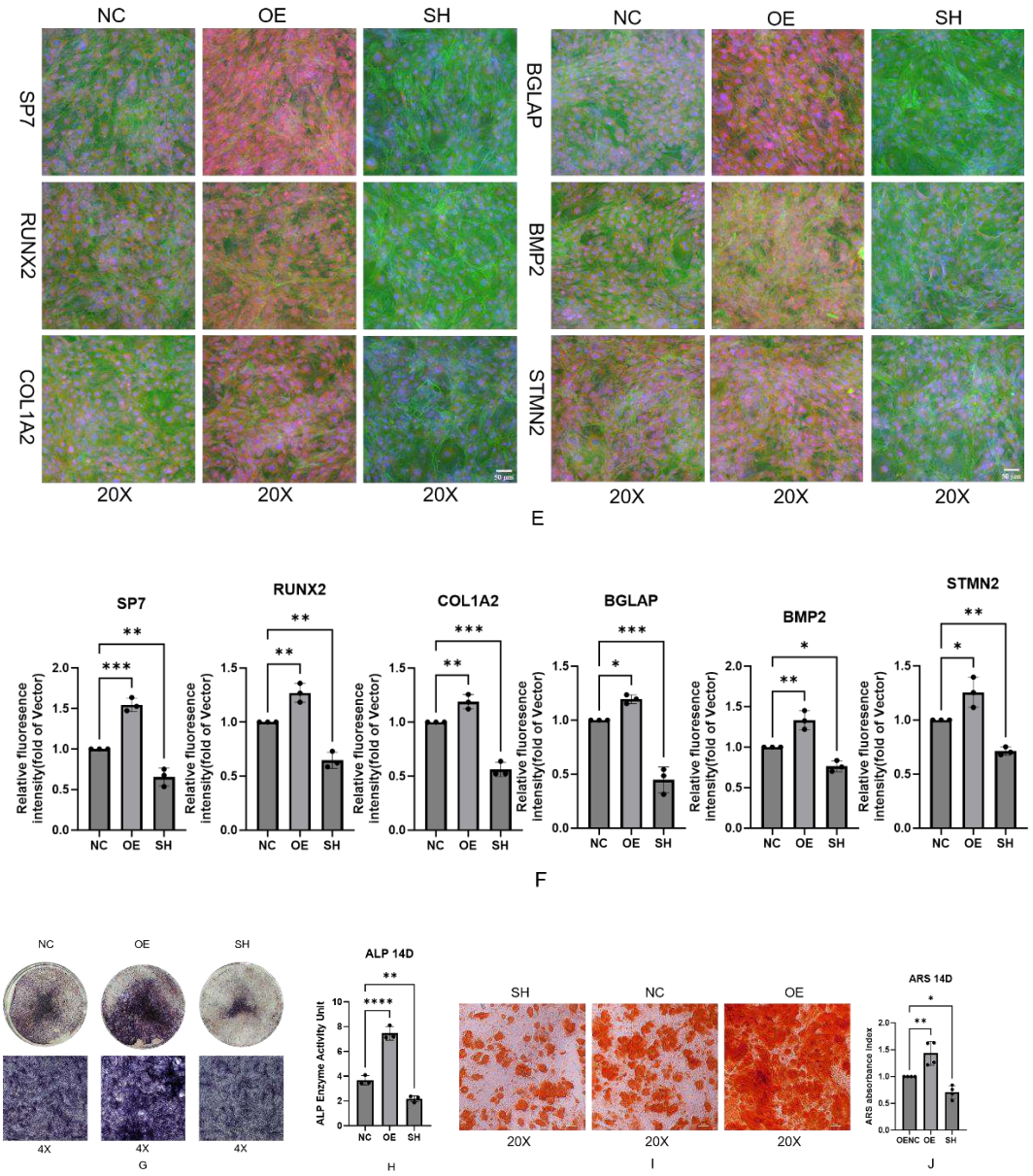
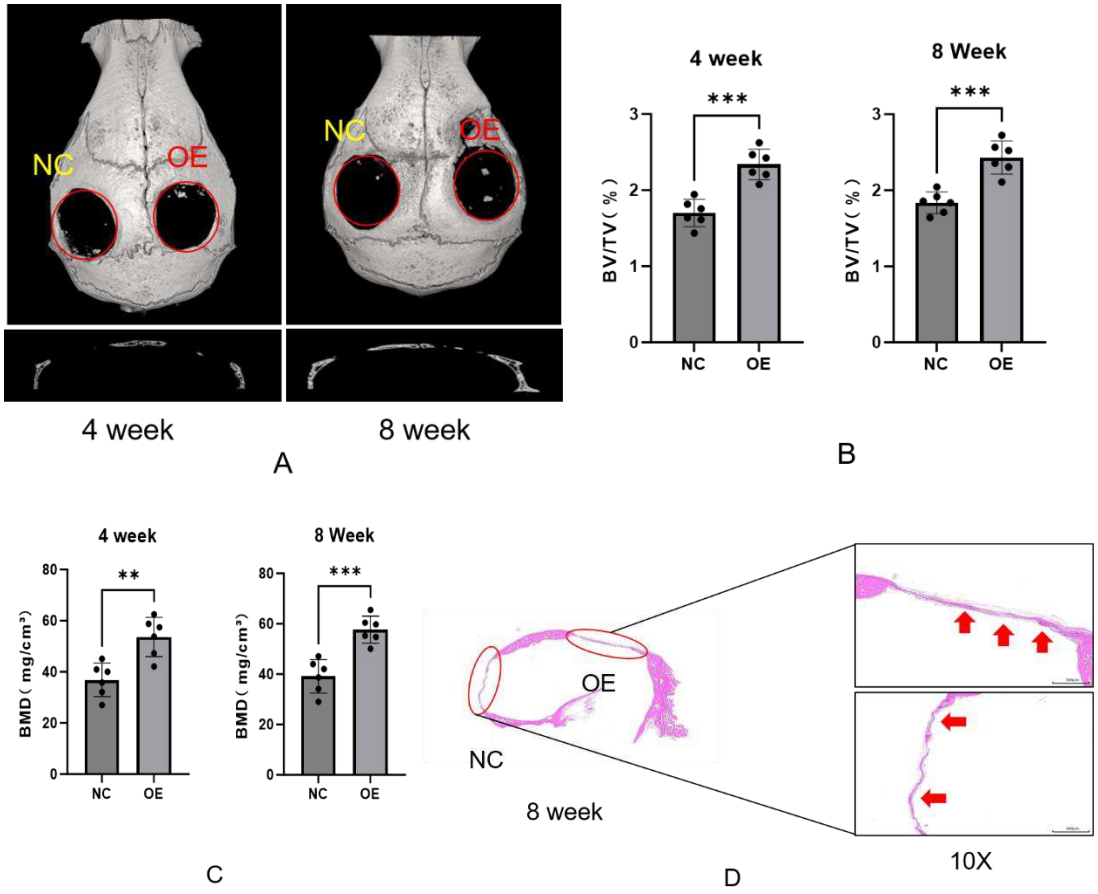


Figure 3. STMN2 enhances osteogenic differentiation and matrix mineralization of BMSCs.

BMSCs were transduced with the indicated lentiviral constructs and cultured in osteogenic induction medium. (A, B) qRT-PCR analysis of BMP2, BGLAP, RUNX2, and COL1A2 mRNA levels in the overexpression (A) and knockdown (B) groups. (C, D) Representative Western blots (C) and densitometric quantification (D) of the corresponding proteins. (E, F) Immunofluorescence staining for osteogenic markers (green) with DAPI nuclear counterstaining (blue) in the overexpression (E) and knockdown (F) groups (scale bars are indicated in the panels). (G, H) ALP staining (G) and quantitative ALP activity (H) on day 14 of induction. (I, J) Alizarin Red S (ARS) staining (I) and quantification of mineralized nodules (J) on day 14. Data are presented as mean ± SD (n = 3 per group). *p < 0.05, **p < 0.01, ***p < 0.001.

2.4. STMN2 accelerates bone regeneration in a mouse calvarial defect model

To further explore the role of STMN2 in bone formation, BMSCs transduced with OE-STMN2 or control lentivirus were implanted into mouse calvarial defects. At 4 and 8 weeks post-implantation, Micro-CT analysis revealed significantly enhanced new bone formation in the overexpression group compared with the NC group (Fig. 4A). Quantitative analysis showed that BV/TV and BMD were significantly higher in the overexpression group (Fig. 4B, C). H&E staining (Fig. 4D) and immunohistochemical staining for RUNX2 and OCN (Fig. 4E) further confirmed increased bone-like tissue formation and osteogenic protein expression in the overexpression group. These results indicate that STMN2 upregulation promotes bone regeneration.



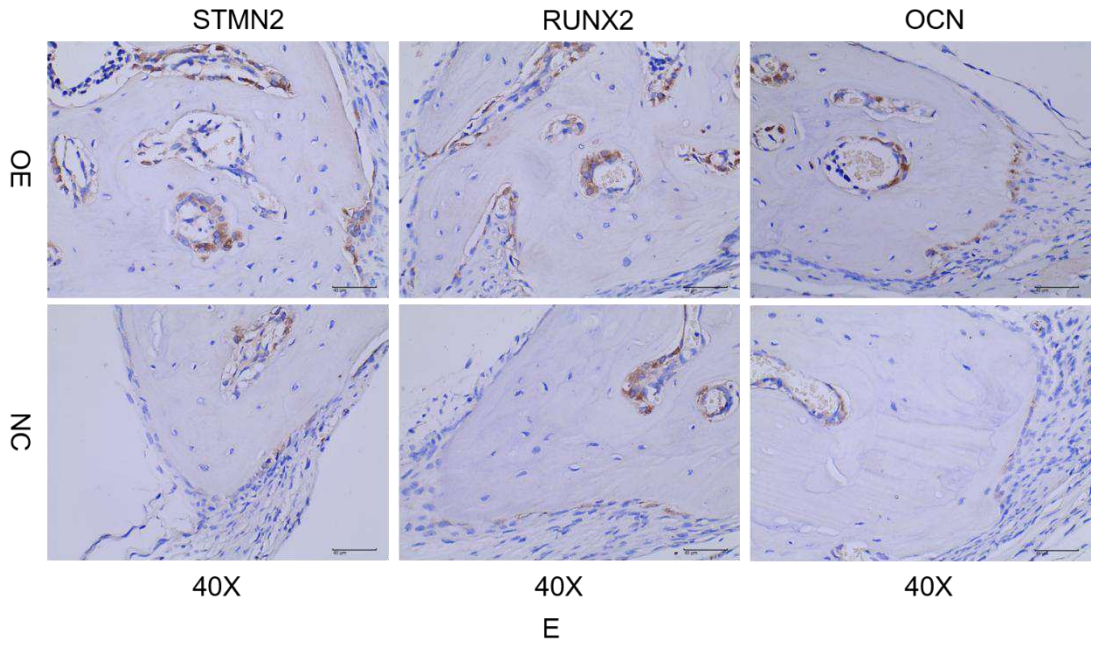


Figure 4. Overexpression of STMN2 promotes bone regeneration in a mouse calvarial defect model. BMSCs transduced with OE-STMN2 or OE-NC lentivirus were implanted into critical-sized calvarial defects in mice. (A) Representative three-dimensional micro-CT reconstructions (coronal and sagittal views) at 4 and 8 weeks post-surgery. (B, C) Quantitative analyses of bone volume/tissue volume (BV/TV) (B) and bone mineral density (BMD) (C) in the defect area. (D) Representative hematoxylin and eosin (H&E) staining of calvarial sections (red arrows indicate newly formed bone-like structures). (E) Representative immunohistochemical staining for STMN2, RUNX2, and OCN (red arrows indicate positively stained cells). Data are presented as mean ± SD (n = 6 per group). *p < 0.05, **p < 0.01, ***p < 0.001.

2.5. STMN2 knockdown inhibits bone regeneration

To further validate the in vivo role of STMN2, BMSCs transduced with SH-STMN2 or control lentivirus were transplanted into calvarial defects. As shown in Fig. 5A, new bone formation was inhibited in the knockdown group compared with the NC group. BV/TV and BMD were both significantly reduced in the knockdown group (Fig. 5B, C). H&E staining (Fig. 5D) and immunohistochemistry for RUNX2 and OCN (Fig. 5E) confirmed that less bone tissue was formed in the knockdown group. These findings further substantiate the positive role of STMN2 in bone regeneration.

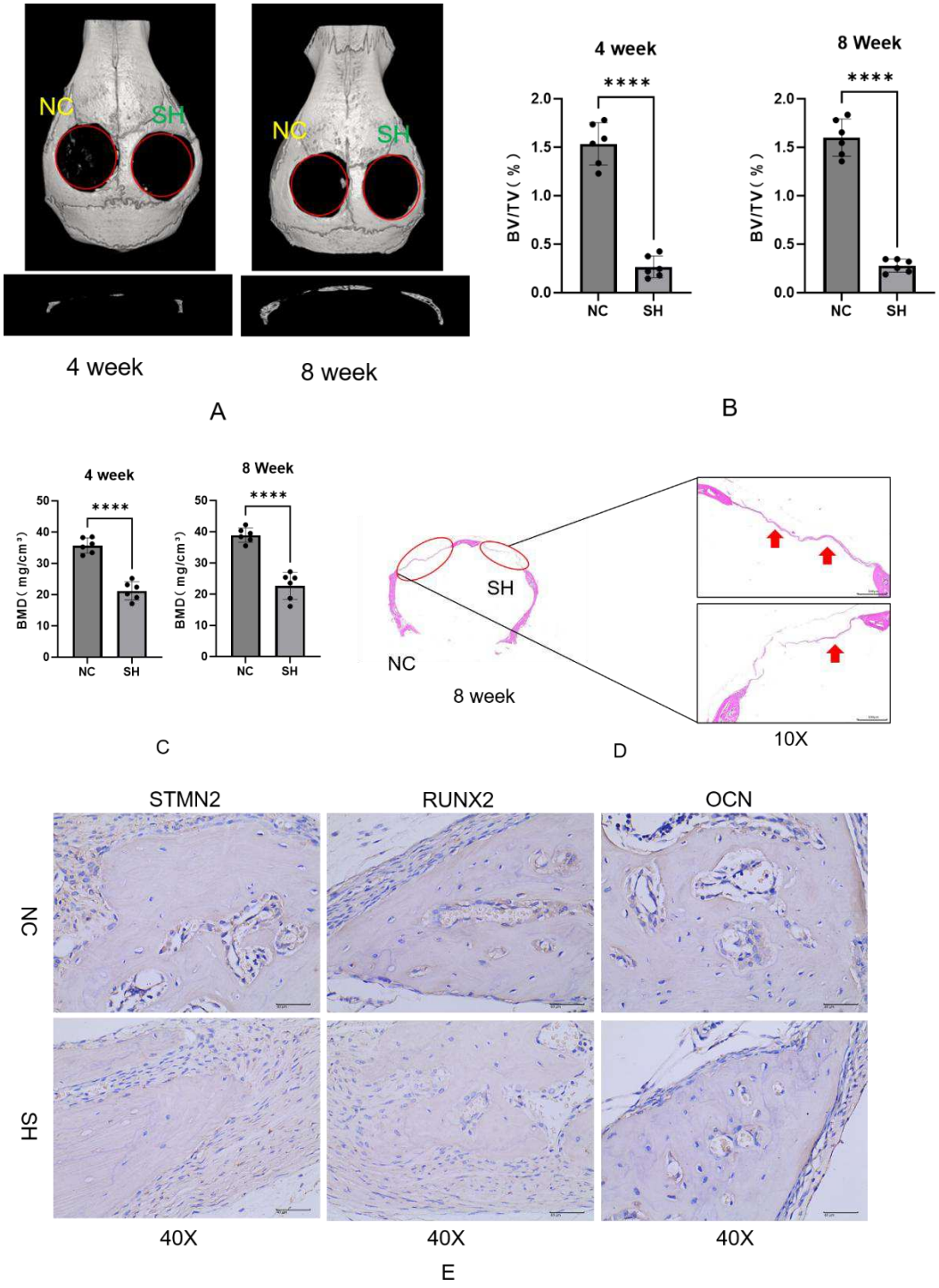


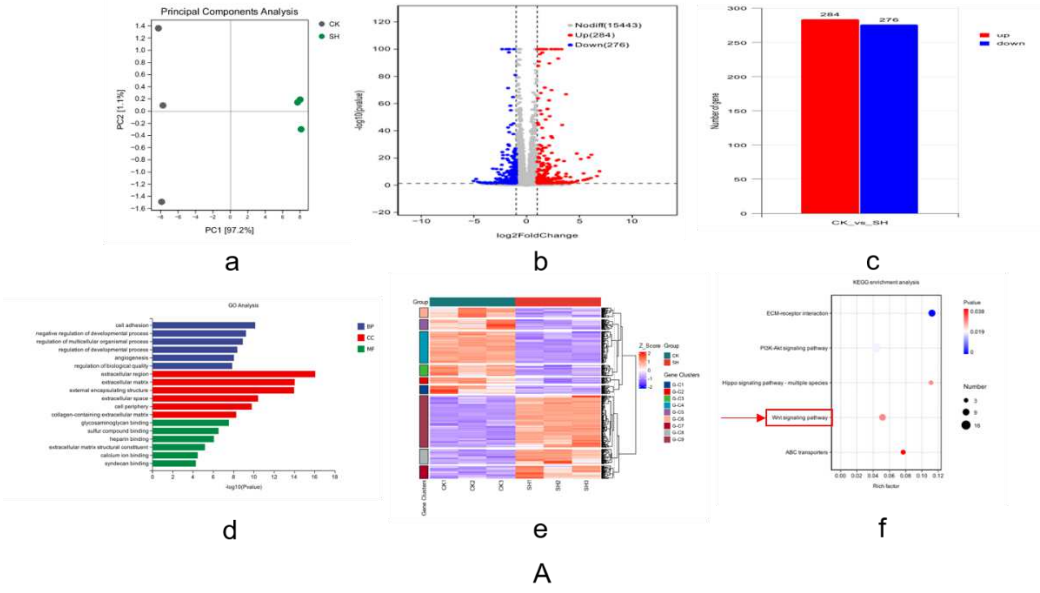
Figure 5. Knockdown of STMN2 impairs bone regeneration in vivo.

BMSCs transduced with SH-STMN2 or SH-NC lentivirus were implanted into calvarial defects. (A) Representative three-dimensional micro-CT reconstructions (coronal and sagittal views). (B, C) Quantitative analyses of BV/TV (B) and BMD (C). (D) Representative H&E staining (red arrows indicate bone-like structures). (E) Representative immunohistochemical staining for STMN2, RUNX2, and OCN (red arrows indicate positively stained cells). Data are presented as mean ± SD (n = 6 per group). *p < 0.05, **p < 0.01.

2.6 STMN2 activates the Wnt/β-catenin pathway in BMSCs

To investigate the underlying molecular mechanism, transcriptome sequencing was performed on BMSCs from the STMN2-knockdown (SH) and NC groups. PCA analysis revealed distinct clustering of gene expression profiles between the two groups (Fig. 6A(a)). Differential expression analysis identified 284 upregulated and 276 downregulated genes (Fig. 6A(b, c)). GO enrichment analysis revealed biological processes such as negative regulation of developmental processes and angiogenesis (Fig. 6A(d)). KEGG pathway enrichment analysis indicated that the differentially expressed genes were associated with the Wnt signaling pathway (Fig. 6A(f)). These findings confirmed the involvement of the Wnt pathway.

To further investigate this mechanism, rescue experiments were performed. Western blot analysis showed that the protein levels of β-catenin, RUNX2, and OCN were lower in the knockdown group, but this effect was partially reversed by treatment with a Wnt pathway agonist (Fig. 6B, C). Similarly, ALP and ARS staining showed that the agonist partially restored the osteogenic differentiation capacity of STMN2-knockdown BMSCs (Fig. 6D–G). Collectively, these results demonstrate that STMN2 promotes osteogenic differentiation of BMSCs, at least in part, through activation of the Wnt/β-catenin signaling pathway.



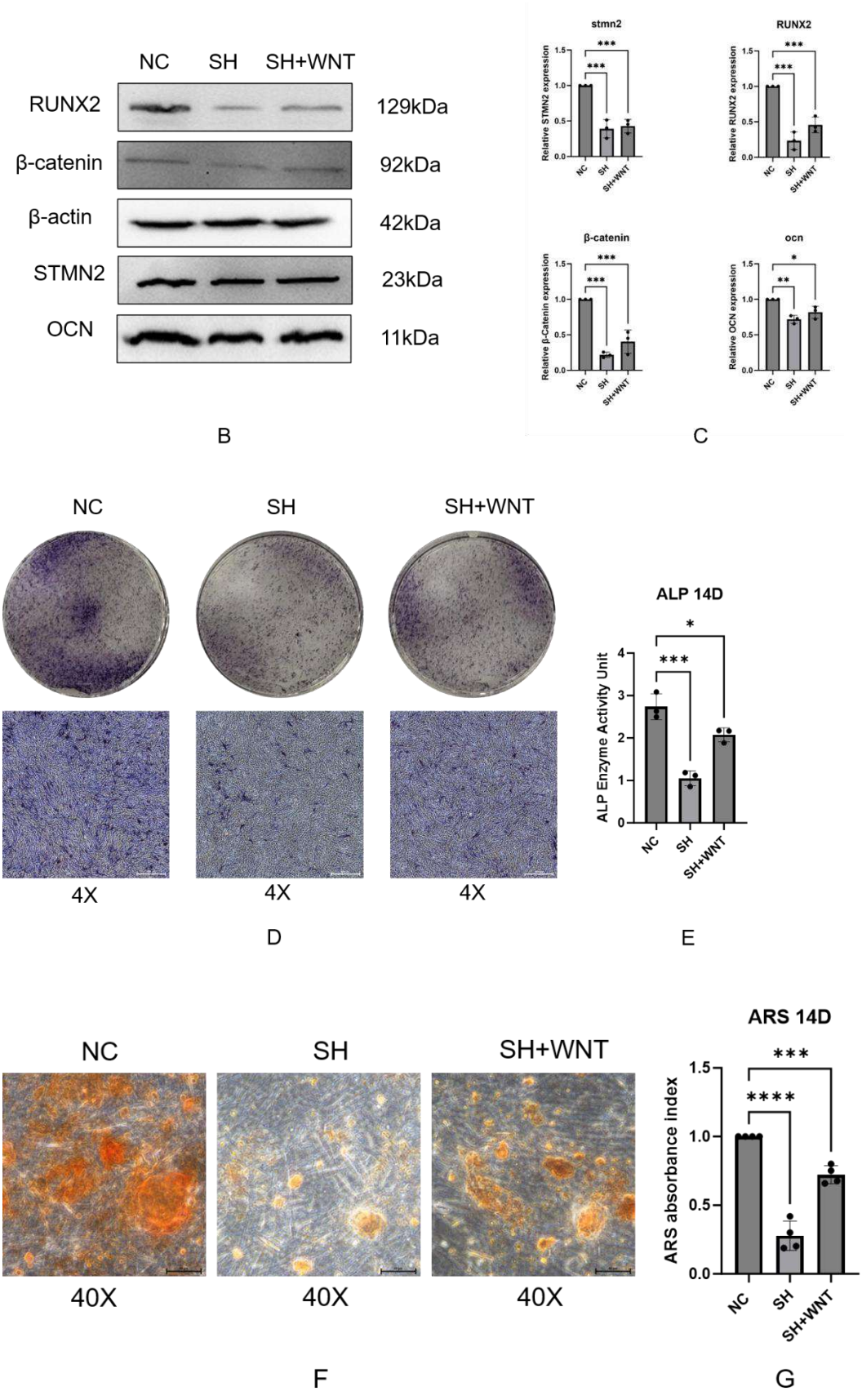


Figure 6. STMN2 modulates osteogenic differentiation via the Wnt/β-catenin signaling pathway.

(A) Transcriptome sequencing analysis of BMSCs from the SH-STMN2 and SH-NC groups. (a) Principal component analysis (PCA) showing distinct clustering of gene expression profiles. (b) Volcano plot of differentially expressed genes. (c) MA plot illustrating 284 upregulated and 276 downregulated genes. (d) Gene Ontology (GO) enrichment analysis. (e) Hierarchical clustering heatmap of differentially expressed genes. (f) Kyoto Encyclopedia of Genes and Genomes (KEGG) pathway enrichment analysis, highlighting the Wnt signaling pathway. KEGG pathway enrichment analysis of differentially expressed genes. The enrichment factor plot shows enriched KEGG pathways based on KEGG annotations. No KEGG pathway map imagery was reproduced. KEGG database references are cited in the main text[28][29][30]. (B–G) Pathway rescue experiments. (B) Representative Western blots of β-catenin, RUNX2, and OCN in SH-NC, SH-STMN2, and SH-STMN2+Wnt agonist groups. (C) Densitometric quantification of the protein bands. (D, E) ALP staining (D) and quantitative activity (E) on day 7 of osteogenic induction. (F, G) ARS staining (F) and quantification of calcium nodules (G) on day 14. Data are presented as mean ± SD (n = 3 per group). *$p < 0.05$, **$p < 0.01$, ***$p < 0.001$; ns, not significant.

3. Discuss

Precise regulation of microtubule dynamics is essential for controlling mesenchymal stem cell (MSC) fate [13]. In the present study, we found that STMN2 expression was markedly upregulated during osteogenic differentiation of BMSCs. Lentivirus-mediated overexpression of STMN2 significantly enhanced BMSC proliferation, migration, osteogenic differentiation, and matrix mineralization, whereas STMN2 knockdown produced opposite effects. Using a mouse calvarial defect model, we confirmed that STMN2 overexpression accelerated new bone formation, while STMN2 knockdown markedly inhibited bone regeneration. Mechanistically, we demonstrated that STMN2 regulates BMSC osteogenic differentiation through activation of the Wnt/β-catenin signaling pathway. These findings reveal a novel role for STMN2 in bone regeneration and identify it as a potential molecular target for BMSC-based bone tissue engineering.

Our observation that STMN2 was upregulated in a time-dependent manner during osteogenic induction is consistent with previous findings. Wang et al. reported STMN2 upregulation in long-term cultured human BM-MSCs[14], and Long et al. identified STMN2 as a gene associated with both neural development and osteogenesis[15]. Kumar et al. detected stathmin in human and rat osteoblasts, suggesting a role for this family in osteoblast function[10]. Furthermore, Chiellini et al[11]. and Tuerlings et al[12].demonstrated STMN2 upregulation during MSC osteogenesis and in osteoarthritic tissues, respectively. Notably, unlike STMN2, STMN1 (stathmin 1) is also upregulated during osteogenic differentiation in various MSCs[16][17][18], suggesting potential functional redundancy or synergy among stathmin family members in osteogenic regulation. This possibility warrants further investigation using double-gene knockout or co-overexpression experiments.

Our gain- and loss-of-function experiments indicated that STMN2 actively and positively regulates osteogenic differentiation. STMN2 overexpression enhanced BMSC proliferation and migration, which are crucial for providing sufficient osteoprogenitor cells and facilitating their recruitment to defect sites. At the differentiation level, STMN2 overexpression increased ALP activity, expression of osteogenic genes (RUNX2, OCN, COL1A1), and matrix mineralization,

while STMN2 knockdown had the opposite effect. These in vitro findings were corroborated in vivo, where the STMN2-overexpressing group exhibited superior bone defect repair in the calvarial model.

Mechanistically, our study demonstrates that STMN2 promotes osteogenic differentiation of BMSCs through activation of the Wnt/β-catenin pathway, a core signaling axis governing BMSC osteogenic differentiation[19][20][21]. Western blot analysis revealed that STMN2 knockdown reduced β-catenin protein levels and nuclear accumulation, accompanied by down regulation of osteogenic transcription factors. Importantly, treatment with a Wnt/β-catenin agonist significantly alleviated the inhibitory effect of STMN2 knockdown on osteogenesis, indicating that the Wnt/β-catenin axis is a critical mediator of STMN2 function. Previous studies have reported that Wnt signaling is activated during the late stages of MSC osteogenic differentiation, coincident with STMN2 upregulation, and STMN2 has been identified as a marker gene of Wnt-mediated osteogenesis, suggesting that STMN2 may act as a downstream target of the Wnt/β-catenin pathway[22]. Additionally, STMN2 has been implicated in the osteogenic differentiation of BMSCs from patients with congenital scoliosis[23]. Collectively, these lines of evidence support that the Wnt/β-catenin pathway constitutes a key molecular mechanism through which STMN2 regulates osteogenic differentiation.

However, the precise molecular linkage between STMN2 and the Wnt/β-catenin pathway remains to be fully elucidated. The microtubule cytoskeleton and Wnt signaling engage in complex bidirectional crosstalk. Wnt signaling can influence microtubule dynamics, while microtubule stability can, in turn, affect the intensity of Wnt signaling by modulating β-catenin trafficking and stability[24][25][26]. As a microtubule-depolymerizing protein, STMN2 may regulate microtubule dynamics, which could then influence β-catenin phosphorylation, degradation, or nuclear translocation. Elucidation of this mechanism will require systematic investigations, including real-time imaging of microtubule dynamics and protein-interaction proteomics.

Although this study systematically reveals a positive regulatory role for STMN2 in BMSC osteogenic differentiation and bone regeneration, several important questions remain. First, the precise molecular linkage by which STMN2 regulates the Wnt/β-catenin pathway requires further elucidation. Second, while the mouse calvarial defect model is a classical system for evaluating bone regeneration, it represents intramembranous ossification. Validation of the therapeutic potential of STMN2 in a more clinically relevant segmental bone defect model of long bones would represent a critical step toward translational application.

In summary, this study identifies a positive regulatory role for STMN2 in the osteogenic differentiation and bone regeneration of BMSCs and demonstrates that STMN2 functions, at least in part, through activation of the Wnt/β-catenin signaling pathway. These findings not only add a novel node to the molecular regulatory network governing bone regeneration but also provide a potential target for optimizing BMSC-based bone tissue engineering strategies. Further investigation of the fine molecular linkage between STMN2 and the Wnt/β-catenin pathway, and evaluation of its therapeutic potential in large-animal bone defect models, will establish a more solid foundation for the treatment of bone metabolic diseases.

4. Materials and Methods

4.1. Experimental animals

All animal procedures were performed in accordance with the institutional guidelines and ethical standards of the Animal Experimentation Ethics Committee of West China Hospital, Sichuan University (approval number: 20250211013). Male C57BL/6J mice (2 and 8 weeks old) were obtained from Sichuan Lilaisinuo Biological Technology Co., Ltd. Animals were housed in a specific-pathogen-free facility under controlled conditions (21 °C, 12-h light/dark cycle) with free access to sterilized water and standard chow. Mice were anesthetized with 2% pentobarbital sodium via intraperitoneal injection at a dose of 50 mg/kg prior to euthanasia. After confirming the loss of consciousness, the mice were euthanized by cervical dislocation.

4.2. Isolation and culture of BMSCs

BMSCs were isolated from the diaphyses of long bones (femur and tibia) of 2–3-week-old C57BL/6 mice using the bone explant adherence method[27]. Briefly, limbs were aseptically harvested, and the surrounding soft tissues were carefully removed. The epiphyseal ends were excised to expose the bone marrow cavity, which was flushed with α-MEM supplemented with 1% penicillin-streptomycin to remove hematopoietic cells. Diaphyseal fragments (1–3 mm) were digested with 1 mg/mL collagenase type I (Solarbio, China) at 37 °C for 60–120 min with gentle agitation. After digestion, the supernatants were discarded, and the bone fragments were thoroughly rinsed with fresh medium. The fragments were then seeded in complete α-MEM containing 10% fetal bovine serum (Procell, China) and 1% penicillin-streptomycin, and cultured under standard conditions (37 °C, 5% CO_2). The medium was first replaced on day 3 post-seeding and every 48 h thereafter. Upon reaching 60–80% confluence, adherent cells were detached using 0.25% trypsin-EDTA (Servicebio, China) and subcultured at a 1:3 ratio. Cells from passages 3 to 5 were used for all experiments.

4.3. Lentiviral transfection

BMSCs in the logarithmic growth phase were seeded into 6-well plates at 2.5×10^5 cells/well and randomly assigned to five groups: STMN2 overexpression (OE-STMN2), overexpression negative control (OE-NC), two independent STMN2 knockdown groups (SH-STMN2-1 and SH-STMN2-2), and knockdown negative control (SH-NC). For transduction, cells were incubated with a viral working solution containing lentiviral particles (Tsingke Biotechnology) and 8 μg/mL polybrene (Tsingke Biotechnology) for 6 h. The viral solution was then aspirated, and cells were washed three times with pre-warmed phosphate-buffered saline (PBS) and cultured overnight in fresh complete medium. Stable transfectants were selected with 8 μg/mL puromycin (Biosharp) starting on day 3 post-infection. Transduction efficiency was confirmed by quantitative real-time PCR (qRT-PCR).

4.4. Induction of osteoblast differentiation

Osteogenic differentiation medium (OriCell, Cat. No. MUXMX-90021) was prepared according to the manufacturer's instructions. Six-well plates were coated with gelatin (OriCell) at room temperature for 30 min, after which the gelatin solution was aspirated and the plates were air-dried. BMSCs were seeded into the coated wells and cultured until appropriate confluence, at which point the medium was replaced with osteogenic induction medium. The medium was renewed every 2–3 days. On day 14 of induction, alizarin red staining was performed to assess mineralized nodule formation.

4.5. Alkaline Phosphatase Staining (ALP) and Activity Assay and Alizarin Red Staining (ARS)

ALP staining was performed on day 14 of osteogenic induction. Briefly, cells were washed three times with PBS, fixed with 2 mL of 4% paraformaldehyde for 30 min at room temperature, and washed again with PBS. The BCIP/NBT working solution was freshly prepared by mixing 3 mL of reaction buffer, 10 μL of BCIP solution, and 20 μL of NBT solution (Beyotime, Cat. No. C3206). Fixed cells were incubated with the working solution in the dark at room temperature for 24 h. After washing with distilled water, stained cells were examined under a light microscope.

ALP activity was assessed on day 14 of induction. Cells were washed with PBS and lysed in 200 μL of RIPA lysis buffer (supplemented with protease inhibitors) on ice for 30 min. Lysates were centrifuged at 12,000 × g for 5 min at 4 °C, and the supernatants were collected. ALP activity was determined using a p-nitrophenyl phosphate (pNPP) colorimetric assay kit (Beyotime, Cat. No. P0321S) following the manufacturer's protocol. Absorbance was measured at 405 nm using a microplate reader.

Alizarin Red S staining was performed on day 14 of induction. Cells were washed with PBS, fixed with 4% paraformaldehyde for 30 min at room temperature, and washed again. Cells were then incubated with Alizarin Red S working solution (OriCell) for 10 min at room temperature. After washing with PBS, stained cells were observed and photographed under a light microscope.

4.6. Cell proliferation assay

BMSCs from each group were harvested and seeded into 96-well plates at 5×10^3 cells/well (five replicate wells per group). PBS was added to the peripheral wells to minimize edge effects. From day 1 to day 5, at the same time each day, 100 μL of complete medium and 10 μL of CCK-8 reagent (Beyotime, Cat. No. C0037) were added to each well. After a 2-h incubation, the absorbance at 450 nm was measured using a microplate reader.

4.7. Cell migration assay

BMSCs were seeded into 6-well plates. At 90–100% confluence, a scratch was made vertically across the monolayer using a sterile 10-μL pipette tip. After washing with PBS to remove detached cells, fresh culture medium was added. Images were captured under an inverted microscope at 0, 12, 24, and 48 h post-scratching. The scratch area was measured using ImageJ software.

4.8. Quantitative RT-PCR

Total RNA was extracted using a commercial kit (Promega, Cat. No. LS1040) according to the manufacturer's instructions. RNA concentration was determined using a Nano-300 microspectrophotometer (Allsheng). Reverse transcription was performed using HiScript IV RT SuperMix for qPCR (+gDNA wiper) (Vazyme, Cat. No. R423-01). Quantitative PCR was carried out with SYBR Green (Toyobo) in triplicate. Mouse β-actin was used as the endogenous reference. Relative expression levels were calculated using the $2^{-}\Delta\Delta Ct$ method. All primer sequences are listed in Table 1.

Table 1: Primer sequence list

Name of gene	Primer sequence
STMN2	FORWARD: CTGTCACTGATCTGCTCCTGCTTC REVERSE: GATCTGCTTCACCTCCATGTCGTC
Beta Actin	FORWARD: CTACCTCATGAAGATCCTGACC REVERSE: CACAGCTTCTCTTTGATGTCAC
RUNX2	FORWARD: CCTTCAAGGTTGTAGCCCTC REVERSE: GGAGTAGTTCTCATCATTCCCG
BMP2	FORWARD: AGTAGTTTCCAGCACCGAATTA REVERSE: CACTAACCTGGTGTCCAATAGT
BGLAP	FORWARD: GGACCATCTTTCTGCTCACTCTGC REVERSE: TCCTGCTTGGACATGAAGGCTTTG
COL1A2	FORWARD: GCCTAGCAACATGCCAATATTT REVERSE: GAATACTGAGCAGCAAAGTTCC

4.9. Western Blotting

Cells were lysed in RIPA buffer supplemented with protease inhibitors (Solarbio). Protein concentration was determined using a BCA protein assay kit (P0012S). Equal amounts of protein were mixed with 5× loading buffer (containing DTT) (Solarbio), heated at 100 °C for 10 min, and separated by SDS-PAGE using 12% polyacrylamide gels (Servicebio, G2178-50T). Electrophoresis was performed at 90 V for 30 min (stacking gel) and 160 V for 60 min (resolving gel). Proteins were transferred onto PVDF membranes (Immobilon) at 400 mA for 60 min using a rapid transfer buffer (Servicebio). Membranes were blocked with 5% non-fat milk (Servicebio) for 60 min at room temperature and incubated with primary antibodies against β-actin (Proteintech, 66009-1-Ig),

STMN2 (Proteintech, 10586-1-AP), BGLAP (ABclonal, A20800), BMP2 (ABclonal, A27101), Collagen I (ABclonal, A21059), and RUNX2 (ABclonal, A11753) overnight at 4 °C. After washing with TBST, membranes were incubated with HRP-conjugated secondary antibodies (Proteintech, RGAR001 and RGAM001) for 1 h at room temperature. Immunoreactive bands were visualized using ECL and captured with the iBright 1500 Imaging System (Thermo Fisher Scientific). Densitometric analysis was performed using ImageJ software.

4.10. Immunofluorescence staining

Cells were washed with PBS, fixed with 4% paraformaldehyde for 30 min, and blocked with 5% sheep serum albumin (Solarbio, SL038) for 1 h at room temperature. Cells were then incubated with primary antibodies against STMN2, SP7, BGLAP, BMP2, Collagen I, and RUNX2 overnight at 4 °C. After washing, cells were incubated with fluorophore-conjugated secondary antibodies (Proteintech, RGAM002 and SA00009-2) for 1 h at room temperature in the dark. Nuclei were counterstained with DAPI for 10 min. Stained cells were examined using a fluorescence microscope (Nikon).

4.11. Animal surgery

Eight-week-old C57BL/6J mice were randomly divided into four groups: OE-STMN2, OE-NC, SH-STMN2, and SH-NC (n = 6 per group). After disinfection of the dorsal head with iodophor, the skin and subcutaneous tissues were incised along the sagittal suture. The skull was exposed, and a circular defect of 3 mm in diameter was created on each side using a skull drill. The cell-Matrigel mixture was gently implanted into the defects, followed by layer-by-layer suturing. At 4 or 8 weeks post-surgery, mice were euthanized by intraperitoneal injection of sodium pentobarbital (10 mg/kg).

4.12. Micro-computed tomography (Micro-CT) analysis

At 4 and 8 weeks post-implantation, skulls were harvested, fixed in 4% paraformaldehyde for 48 h, and analyzed using a micro-CT imaging system (SkyScan1276, Bruker, Kontich, Belgium). Scanning parameters were as follows: voltage 85 kV, current 200 μA, resolution 6.5 μm, rotation angle 0.3° (360° scan), exposure time 450 ms, and Al filter 1 mm. Reconstruction was performed using NRecon software, and three-dimensional structural parameters were analyzed using CTAn software (Bruker). Bone volume/tissue volume (BV/TV) and bone mineral density (BMD) were calculated.

4.13. Hematoxylin and eosin (H&E) staining

After micro-CT analysis, skull samples were fixed, decalcified, embedded in paraffin, and sectioned. Sections were deparaffinized, rehydrated, stained with hematoxylin (Solarbio) for 5–10

min, rinsed, differentiated in acid-alcohol solution, and blued in weak alkaline solution. Sections were then stained with eosin (Solarbio) for 3 min, dehydrated, cleared, and mounted.

4.14. Immunohistochemistry

Paraffin-embedded sections were deparaffinized, rehydrated, and subjected to antigen retrieval. Endogenous peroxidase activity was blocked, and sections were incubated with primary antibodies against STMN2 (Proteintech, 10586-1-AP), OCN (Proteintech, 23418-1-AP), and RUNX2 (Proteintech, 20700-1-AP) overnight at 4°C. After washing, sections were incubated with secondary antibody (Proteintech, RGAR011), and immunoreactivity was visualized using DAB (Proteintech, PR30018). Sections were counterstained, dehydrated, and mounted.

4.15. Transcriptome Sequencing (RNA-seq)

BMSCs transduced with SH-STMN2 or SH-NC lentivirus were subjected to osteogenic induction (three biological replicates per group). At 80% confluence, total RNA was extracted using TRIzol reagent. RNA concentration, purity, and integrity were assessed. Library construction and sequencing were performed by Shanghai Personal Biotechnology Co., Ltd.

4.16. Pathway rescue experiment

BMSCs transduced with SH-NC or SH-STMN2 lentivirus were divided into three groups: SH-NC, SH-STMN2, and SH-STMN2 + agonist. The Wnt/β-catenin agonist 4 (Solarbio) was added at a final concentration of 100 μmol/L for 6 h, after which the medium was replaced with osteogenic induction medium. At day 7, ALP staining and activity assay were performed; at day 14, ARS staining and quantification were performed. The experiment was repeated three times.

4.17. Statistical analysis

Data are presented as mean ± standard deviation (SD). Comparisons between two groups were performed using Student's t-test, while comparisons among three or more groups were performed using one-way analysis of variance (ANOVA). All experiments were repeated at least three times. A p-value < 0.05 was considered statistically significant. Significance levels are indicated as *$p < 0.05$, **$p < 0.01$, ***$p < 0.001$, and ****$p < 0.0001$; ns, not significant.

Data availability

The datasets generated and/or analyzed during the current study are available in the NCBI Sequence Read Archive (SRA) repository under BioProject accession number PRJNA1540018. The

data is publicly accessible at https://www.ncbi.nlm.nih.gov/sra/PRJNA1540018.

References

[1]. Wang, Z. et al. Promoting bone generation through the accordion technique in critical-sized bone defects: a review. *Int. J. Surg.* **111**, 8423–8434 (2025).

[2]. Meshry, N. & Carneiro, K. M. M. DNA as a promising biomaterial for bone regeneration and potential mechanisms of action. *Acta Biomater.* **197**, 68–86 (2025).

[3]. Ivanova, N. et al. Types of bone substitutes and their application in regenerative medicine: a systematic review. *J. Funct. Biomater.* **16**, 341 (2025).

[4]. Yu, D. et al. Treatment of large bone defects in load-bearing bone: traditional and novel bone grafts. *J. Zhejiang Univ. Sci. B* **26**, 421–447 (2025).

[5]. Zhang, L. et al. Engineered 3D mesenchymal stem cell aggregates with multifunctional prowess for bone regeneration: current status and future prospects. *J. Adv. Res.* **79**, 409–431 (2026).

[6]. Qi, J. et al. Current biomaterial-based bone tissue engineering and translational medicine. *Int. J. Mol. Sci.* **22**, 10233 (2021).

[7]. Baughn, M. W. et al. Mechanism of STMN2 cryptic splice-polyadenylation and its correction for TDP-43 proteinopathies. *Science* **379**, 1140–1149 (2023).

[8]. Klim, J. R. et al. Connecting TDP-43 pathology with neuropathy. *Trends Neurosci.* **44**, 424–440 (2021).

[9]. Thornburg-Suresh, E. J. C. & Summers, D. W. Microtubules, membranes, and movement: new roles for stathmin-2 in axon integrity. *J. Neurosci. Res.* **102**, e25382 (2024).

[10]. Kumar, R. & Haugen, J. D. Human and rat osteoblast-like cells express stathmin, a growth-regulatory protein. *Biochem. Biophys. Res. Commun.* **201**, 861–865 (1994).

[11]. Chiellini, C. et al. Stathmin-like 2, a developmentally-associated neuronal marker, is expressed and modulated during osteogenesis of human mesenchymal stem cells. *Biochem. Biophys. Res. Commun.* **374**, 64–68 (2008).

[12]. Tuerlings, M. et al. RNA sequencing reveals interacting key determinants of osteoarthritis acting in subchondral bone and articular cartilage: identification of IL11 and CHADL as attractive treatment targets. *Arthritis Rheumatol.* **73**, 789–799 (2021).

[13]. Shi, H. et al. Integrating physicomechanical and biological strategies for BTE: biomaterials-induced osteogenic differentiation of MSCs. *Theranostics* **13**, 3245–3275 (2023).

[14]. Wang, S. et al. Effects of long-term culture on the biological characteristics and RNA profiles of human bone-marrow-derived mesenchymal stem cells. *Mol. Ther. Nucleic Acids* **26**, 557–574 (2021).

[15]. Long, Q. et al. Single-cell RNA and ATAC sequencing reveals cell subsets characteristics in adipose-derived stem cells. *Biochim. Biophys. Acta Mol. Cell Biol. Lipids* **1871**, 159734(2026).

[16]. Shang, J. et al. Hyperlipidemia impairs bone repair and regeneration via miR-193a-3p/STMN1/PI3K/Akt axis. *Biochem. Pharmacol.* **232**, 116693 (2025).

[17]. Sun, J. et al. Long noncoding RNA AC092155 facilitates osteogenic differentiation of adipose-derived stem cells through the miR-143-3p/STMN1 axis. *J. Gene Med.* **23**, e3363(2021).

[18]. Sauer, T. et al. Protein expression of AEBP1, MCM4, and FABP4 differentiate osteogenic,

adipogenic, and mesenchymal stromal stem cells. *Int. J. Mol. Sci.* **23**, 2568(2022).
[19]. Zhu, S. et al. Cell signaling and transcriptional regulation of osteoblast lineage commitment, differentiation, bone formation, and homeostasis. *Cell Discov.* **10**, 71(2024).
[20]. Hu, L. et al. Wnt/β-catenin signaling components and mechanisms in bone formation, homeostasis, and disease. *Bone Res.* **12**, 39(2024).
[21]. Maurice, M. M. & Angers, S. Mechanistic insights into Wnt-β-catenin pathway activation and signal transduction. *Nat. Rev. Mol. Cell Biol.* **26**, 371–388 (2025).
[22]. Guo, P. et al. A single-cell transcriptome of mesenchymal stromal cells to fabricate bioactive hydroxyapatite materials for bone regeneration. *Bioact. Mater.* **9**, 281–298 (2021).
[23]. Zheng, Y. et al. WISP2 downregulation inhibits the osteogenic differentiation of BMSCs in congenital scoliosis by regulating Wnt/β-catenin pathway. *Biochim. Biophys. Acta Mol. Basis Dis.* **1869**, 166783(2023).
[24]. Kumari, A. et al. Microtubule-targeting agents impair kinesin-2-dependent nuclear transport of β-catenin: evidence of inhibition of Wnt/β-catenin signaling as an important antitumor mechanism of microtubule-targeting agents. *FASEB J.* **35**, e21539(2021).
[25]. Puri, D. et al. Wnt signaling establishes the microtubule polarity in neurons through regulation of Kinesin-13. *J. Cell Biol.* **220**, e202005080(2021).
[26]. Habib, S. J. & Acebrón, S. P. Wnt signalling in cell division: from mechanisms to tissue engineering. *Trends Cell Biol.* **32**, 1035–1048 (2022).
[27]. Zhu, H. et al. A protocol for isolation and culture of mesenchymal stem cells from mouse compact bone. *Nat. Protoc.* **5**, 550–560 (2010).
[28]. Kanehisa, M. and Goto, S. KEGG: Kyoto Encyclopedia of Genes and Genomes. *Nucleic Acids Res.* **28**, 27–30 (2000).
[29]. Kanehisa, M. Toward understanding the origin and evolution of cellular organisms. *Protein Sci.* **28**, 1947–1951 (2019).
[30]. Kanehisa, M., Furumichi, M., Sato, Y., Ishiguro-Watanabe, M., and Tanabe, M. KEGG: integrating viruses and cellular organisms. *Nucleic Acids Res.* **49**, D545–D551 (2021).

Acknowledgements

The authors wish to thank all the teachers who contributed to this study for their invalu able help and support. This study was supported by a Grant-in-Aid (No. 2023YFS0235) o btained from the Science and Technology Department of Sichuan Province.

Funding

This study was supported by a Grant-in-Aid (No. 2023YFS0235) obtained from the Scie nce and Technology Department of Sichuan Province.

Author contributions

Zhangzheng D designed the research. Xiaoping J conducted the experiment, wrote the m anuscript, performed data analysis and interpretation. Shuxing X provided materials. Jun C and Zhangzheng D proofed and revised the manuscript. All authors read and approved the final manuscript.

Affiliations

Xiaoping Jin[1,2] Jun Cheng[2], Shuxing Xing[2]*, Zhangzhen Du[2]**.

1.Chengdu University of Traditional Chinese Medicine, Chengdu 611137, China.

2. Department of Orthopaedics, Chengdu Fifth People's Hospital, Chengdu 611130, China.

*Corresponding author at: Department of Orthopaedics, Chengdu Fifth People's Hospital, Chengdu 611130, China.

**Corresponding author at: Department of Orthopaedics, Chengdu Fifth People's Hospital, Chengdu 611130, China.

E-mail addresses: 3296315867@qq.com(S. Xing), dzzupu@163.com(Z. Du)

Competing interests

The authors declare no competing interests.

Ethics approval

All animal procedures were reviewed and approved by the Animal Ethical Approving C ommittee of West China Hospital, Sichuan University (Approval No. 20250211013). All ex periments were conducted in accordance with the relevant ethical guidelines and standards for the care and use of laboratory animals.

Supplementary Files

This is a list of supplementary files associated with this preprint. Click to download.

- SupplementaryInformation.docx